HHS Public Access

Author manuscript

J Neurosci Methods. Author manuscript; available in PMC 2024 May 15.

Published in final edited form as:

J Neurosci Methods. 2023 May 15; 392: 109867. doi:10.1016/j.jneumeth.2023.109867.

A novel 4-cell in-vitro blood-brain barrier model and its characterization by confocal microscopy and TEER measurement

Johid R. Malik[1], **Courtney V. Fletcher**[1,3], **Anthony T. Podany**[1], **Shetty Ravi Dyavar**[2], **Kimberly K. Scarsi**[1,3], **Gwendolyn M. Pais**[4,5], **Marc H. Scheetz**[4,5], **Sean N. Avedissian**[#,1]

[1]Antiviral Pharmacology Laboratory, College of Pharmacy. University of Nebraska Medical Center. Omaha, NE, USA.

[2]Adicet Bio, Redwood City, CA. 94025

[3]Division of Infectious Diseases, Department of Medicine, University of Nebraska Medical Center. Omaha, NE, USA

[4]Department of Pharmacy Practice, Chicago College of Pharmacy, Midwestern University, Downers Grove, Illinois, USA

[5]Midwestern University, College of Pharmacy Center of Pharmacometric Excellence, Downers Grove, Illinois, USA

Abstract

The blood-brain barrier (BBB) is a protective cellular anatomical layer with a dynamic microenvironment, tightly regulating the transport of materials across it. To achieve in-vivo characteristics, an in-vitro BBB model requires the constituent cell types to be layered in an appropriate order. A cost-effective in-vitro BBB model is desired to facilitate central nervous system (CNS) drug penetration studies. Enhanced integrity of tight junctions observed during the in-vitro BBB establishment and post-experiment is essential in these models. We successfully developed an in-vitro BBB model mimicking the in-vivo cell composition and a distinct order of seeding primary human brain cells. Unlike other in-vitro BBB models, our work avoids the

[#]**Corresponding Author Contact Information:** Sean N Avedissian, PharmD, MS, Antiviral Pharmacology Laboratory, University of Nebraska Medical Center, 986145 Nebraska Medical Center, Omaha, NE 68198-6145, Sean.avedissian@unmc.edu.

Declarations of interest: none

Credit Author Statement

Johid R. Malik: Conceptualization, Methodology, Writing - Original Draft, Writing - Review & Editing, Formal analysis.
Courtney V. Fletcher: Conceptualization, Writing - Review & Editing, Funding acquisition, Validation, Project administration.
Anthony T. Podany: Writing - Review & Editing, Validation, Project administration
Shetty Ravi Dyavar: Conceptualization, Methodology, Writing - Review & Editing.
Kimberly K. Scarsi: Writing - Review & Editing.
Gwendolyn M. Pais: Writing - Review & Editing.
Marc H. Scheetz: Writing - Review & Editing.
Sean N Avedissian: Supervision, Visualization, Writing - Review & Editing, Resources, Funding acquisition, Validation, Project administration

need for pre-coated plates for cell adhesion and provides better cell visualization during the procedure. We found that using bovine collagen-I coating, followed by bovine fibronectin coating and poly-L-lysine coating, yields better adhesion and layering of cells on the transwell membrane compared to earlier reported use of collagen and poly-L-lysine only. Our results indicated better cell visibility and imaging with the polyester transwell membrane as well as point to a higher and more stable Trans Endothelial Electrical Resistance values in this plate. In addition, we found that the addition of zinc induced higher claudin 5 expressions in neuronal cells. Dolutegravir, a drug used in the treatment of HIV, is known to appear in moderate concentrations in the CNS. Thus, dolutegravir was used to assess the functionality of the final model and cells. Using primary cells and an in-house coating strategy substantially reduces costs and provides superior imaging of cells and their tight junction protein expression. Our 4-cell-based BBB model is a suitable experimental model for the drug screening process.

Keywords

in-vitro model; blood-brain-barrier; central nervous system

Materials and methods:

Cells and Culture system

Human brain primary astrocytes (#1800), pericytes (#1200), and human brain microvascular endothelial cells (hBMECs # 1000) were purchased from ScienCell Research Laboratories (SCRL), USA. Required media and growth supplements for the respective cells were also obtained from SCRL. Astrocytes were cultured in astrocyte media (AM) (Catalogue # 1801) and astrocyte growth supplement (AGS) (Catalogue # 1852); Pericytes were cultured in Pericyte media (PM) (Catalogue # 1201), Pericyte growth supplement (PGS) (Catalogue # 1252); hBMECs were cultured in Endothelial cell medium (ECM) (Catalogue # 1001), endothelial growth supplement (ECGS) (Catalogue # 1052), all procured from SCRL. Supplements including FBS (Catalogue # 0010), and penicillin/streptomycin solution (P/S) (Catalogue # 0503) were also purchased from SCRL. Frozen cells were revived and cultured according to the manufacturer's instructions. Cells were grown in either $25cm^2$, $75cm^2$, or $150cm^2$ culture flask (TPP # 90076) in accordance with experimental requirements. For human brain cells, culturing flasks and plates were pre-coated with bovine fibronectin at 2μg/ml (SCRL, # 8248). Approximately 90% of cells in a confluent flask were harvested by trypsinization (0.25 % trypsin, Lonza # CC-5012) and washed in DPBS (Dulbecco's # 1960454). Cells were prepared for counting by mixing 10 μl of cell suspension with 10 μl of trypan blue. 10 μl of the mixture was read in a cell counter (Invitrogen Countess). Cells from passage number 5-8 were used as needed for experimental procedures. Human neuronal cells were also purchased from SCRL (catalogue# 1520), thawed and used on the day of experiment without prior culturing.

Model Optimization

Our model was based on the initial methodology established by Stone et al and previous models by Hind et al, and Allen et al[1-3]. However, we modified the model given the current

availability of necessary supplies, specifically collagen coated inserts of 3.0 μm and 12 mm (no longer available). Further, we performed numerous preliminary experiments, including the stepwise addition of each cell type to confirm cell organization (data not shown).

Transwell Plates and Coating

Twelve-well polycarbonate and polystyrene transwell insert plates (12mm, 3 μm pore) were purchased from Corning (Corning COSTAR, #3402 and 3462). In consecutive treatments, the transwell membrane was coated with bovine collagen I (Gibco, #A10644-01), fibronectin, and poly-L-Lysine. Briefly, the membrane was initially treated with bovine collagen I (50μg/ml, Gibico, #A10644-01) in PBS overnight at 4°C. Next, fibronectin (ScienCell, #8248) 3μg/ml in PBS was added to the transwell membrane and incubated at 37°C for 3hrs. The membrane was left to air dry between treatments. Finally, Poly-L-Lysine (Sigma, #P4707-50ML) was added to the membrane and incubated for 10 minutes at room temperature (RT).

Cell Seeding on Transwell Membrane

The experimental timeline is described in Figure 1. All steps were carried out in a biosafety cabinet under aseptic conditions.

Astrocytes (1st cell)-Astrocytes with a cell count of 6x10^5/150μl, 3x10^5/150μl, and 1.5x10^5/150μl were seeded on the basolateral side of the flipped transwell insert membranes and incubated in 37°C cell culture for 3 hrs. After the incubation, excess media was removed, flipped to the original position, and media was added to the wells covering the apical compartment. Astrocytes were grown for 48 hrs.

Pericytes (2nd cell)-After 48 hrs of incubation with astrocytes, the transwell was flipped again, and excess media was removed from the top of the monolayer. Keeping the ratio 1:5 for astrocyte: pericytes, 1.2x10^5/150μl, 0.6x10^5/150μl, and 0.12x10^5/150μl of pericytes were seeded on the growing astrocytes monolayer on the basolateral side of the transwell insert membrane. These pericyte-seeded transwells were incubated for 3 hrs in the cell incubator. After the incubation period, the inserts were flipped to normal position, and excess media was removed from the membrane. A 1:1 proportion mixture of astrocyte/pericyte media was filled into the transwell and incubated for five additional days to allow the formation of a confluent monolayer of astrocytes and pericytes. The media was changed every 48 hrs.

hBMECs (3rd cell) and Neuron (4th cell) Seeding-Seven days after the initial seeding with astrocytes, the apical layer media was removed, and 7.51x10^4/200μl hBMECs in endothelial media were seeded on the transwell membrane containing astrocytes and pericytes (6x10^5/150μl and 1.2x10^5/150μl), in the basolateral part. Plates with seeded cells were incubated for 6 hours, and then 400μl of endothelial media was added to the apical region of the transwell membrane. In parallel, 200μl of 2.5x10^4 human neurons were seeded on a collagen-coated coverslip in a separate 12-well plate and incubated for 2 hours. The media was changed every 48 hours.

Combining all Four Cells- On the 11th day from initiation of the experiment, the transwell inserts with apical hBMECs, and basolateral astrocyte and pericytes were carefully

transferred to the 12-well plate containing neurons on the coverslip at the bottom of the well. The apical side of the transwell was topped with fresh endothelial media, while the basolateral part was filled with a 1:1:2 ratio of astrocyte, pericyte, and neuronal media.

Trans Epithelial Electrical Resistances (TEER) Measurements

Before changing the media on Day 3 of 4-cell growth, the first TEER value was measured using an EVOM^2 meter (Epithelial volt-ohm meter). EVOM^2 has been specifically designed to measure the electrical resistance in tissue culture (https://www.wpiinc.com/company/our-history/). The instrument precisely measures the electrical resistance between the different layers of cells. The measured electrical resistance between tissue layers is usually known as TEER. The resistance measuring probe was washed in 70% ethanol and dried before equilibrating in endothelial media for 15 minutes. After equilibration, the probe was carefully placed into the insert with the shorter arm just above the hBMECs (apical) layer and the long arm just above the neurons on the coverslip at the bottom of the well. TEER value was checked every day until the completion of the experiment.

Processing Transwell Membrane

Upon completion of the experiment, wells with the membrane inserts were washed twice with PBS, and the cells were fixed with paraformaldehyde (Thermo Scientific, #J19943-K2) for 10 minutes. Fixed membranes with cells were washed with PBS, and the membrane-containing cells were carefully cut into four pieces for further staining.

Staining Cells on the Membranes for Imaging

A piece of the membrane containing cells on both sides was incubated in a blocking buffer comprising 5% goat serum (Abcam, #ab7481), 0.1% TritonX 100 (Sigma, # 9036-19-5), and 1% BSA (MP, #180561) for 2 hours. Cells were washed in PBS with 0.1% Tween-20 (Sigma, #P2287-100ML). Conjugated antibodies for claudin 5 (Invitrogen, #362588) at 1:200 and ZO-1 (Invitrogen, #MA3-39100-A647) at 1:100 dilution in PBS with 0.1% Tween-20 were added to the samples and incubated overnight at 4°C. A separate piece of the same membrane was used for cell identification by staining it with cell marker conjugated-antibodies, anti-S1OO beta for astrocytes (Abcam, #ab196175), anti-CD146 (Abcam, #ab196448) for pericytes and hBMECs, and anti-NeuN antibody (Abcam, ab190565) for neurons, with all Abs at 1:200 dilution. The following day, samples were washed twice with PBS and 0.1% Tween-20. After washing, samples were fixed with 4% paraformaldehyde for 10 minutes in the dark. The fixed samples were washed with PBS and air-dried on a glass cover slip. Samples were analyzed for expression of tight junction proteins using a laser scanning microscope (Zeiss LSM800). Of note, no quantification of fluorescence intensities for proteins was performed and comparison of fluorescence was assessed visually.

Apical and Basolateral Visualization of Cells on the Same Membrane

For optimal visualization of cells on both sides of the membrane, one drop of nucleus staining DAPI (4',6-diamidino-2-phenylindole) mounting dye (Invitrogen-ProLong™Diamond Antifade Mountant with DAPI, #P3692) was added on a glass coverslip. A quarter piece of the air-dried membrane was placed on the DAPI drop, and a drop of

DAPI mounting dye was added on top of the membrane. Finally, another glass coverslip was carefully placed.

Quantification of fluorescence intensity

The confocal images were analyzed for their respective fluorescence pixel intensity by importing the images into Fiji ImageJ software for image analysis[4, 5]. We selected the visually brightest cell in each sample as a representative of the triplicates of each BBB type. The image analysis program calculated the whole cell surface area for mean fluorescence intensity (MFI). Black background or no cell region MFI was also obtained using the same selected cell area and was subtracted from the cell MFI for the final MFI. The software delivers the mean intensity for the entire area selected.

Functional Evaluation of the 4-cell Model with Drug Penetration Analysis

Dolutegravir (DTG) is an integrase strand transfer inhibitor commonly used in antiretroviral therapy (ART) to treat infection with the human immunodeficiency virus (HIV). Here, DTG was utilized as a control to show the functionality of the model. We mixed the corresponding media mentioned above with 4000ng/ml of DTG dissolved in vehicle [Dimethyl sulfoxide (DMSO)/Polyethene glycol-400 (PEG400)/Propylene glycol (PG)/ethanol/kolliphor/1× PBS (8/25/15/10/7/35% v/v)]. The drug-containing media was then added to the apical layer of the transwell membrane. A total of 2000 ng DTG in 0.5ml media was added to the apical layer of BBB. After 48 hours of drug treatment, 0.5ml of media from the apical and basal layer was collected and preserved at −70° for further analysis. The concentration of DTG in the collected media was analyzed using validated LC/MS/MS methodology previously described[6-8].

Introduction

The blood-brain barrier (BBB) represents a dynamic microenvironment where the transport of molecules into and out of the brain is tightly regulated[9]. The unique structure of the BBB is maintained primarily by brain microvascular endothelial cells (BMECs), astrocytes, pericytes, and neuronal projections. Cell-to-cell contact and communication among BMECs, astrocytes, pericytes, and neuronal cells are critical for the integrity and effective functioning of the BBB. The BBB is important as it regulates paracellular exchange, cytoplasmic intake, and exocytosis of essential molecules[9, 10]. Claudins, occludins, and junctional adhesion molecules (JAMs) form tight junctions between cells in the BBB. Cytoplasmic zonula occludens protein 1 and 2 (ZO-1, ZO-2) play vital roles in linking the transmembrane proteins to actin filaments of the cytoskeleton[11]. Together, the tight junction complexes and participating proteins ensure the regulated transport of molecules across the BBB[12]. During a homeostatic condition, only small molecules (molecular mass <400-500 Da) can cross the BBB without needing any modulation of the barrier[13]. Most drugs used to treat disorders of the central nervous system (CNS) need specific properties to cross the BBB. However, a study that looked at over 7000 drugs found that less than 5% of the screened drugs were able to effectively cross BBB, showcasing the significance of this potential obstacle in the brain tissue penetrating drug development process[14].

It is essential to understand the structural and functional aspects of the BBB for the success of CNS drug delivery. It has been debated that relying on the rodent BBB models does not provide critical answers on the human BBB as there are significant differences between species based on transporter expression, the complexity of tight junctions, and drug receptors[15-19]. Species-dependent variations in BBB function has been reported in a positron emission tomography (PET) study on brain pharmacokinetics of a P-glycoprotein (P-gp) substrate[20]. Thus, in-vitro humanized BBB models are crucial experiments and methodologies to understand drug transport across the human BBB. Furthermore, there is a distinct movement towards animal reduction in pre-clinical testing[21]. The 117th U.S. Congress approved the non-requirement of animal testing for procuring a license. Accordingly, FDA no longer has to require animal testing for toxicology data and encourages readily available in-vitro based experiments[22, 23].

In-vitro BBB models are based on the transwell apparatus, which closely mimics in-vivo barrier properties[24, 25]. This method is also cost-effective for screening a large number of drug candidates. Since the incorporation of endothelial cells on a transparent collagen filter, transwell technology has advanced significantly to make it more suitable for BBB studies[26, 27]. Initially, experiments using immortalized brain endothelial cells (BECs) were performed to understand the complexity and functionality of the human BBB[28, 29]. Despite the successful monolayer BBB model on the transwell membrane, cross-talk between different cell types was not possible given the simplicity of the model[30]. Although easily accessible and highly reproducible, the immortalized cells demonstrate poor BBB properties and lose important in-vivo BBB functions[31, 32]. To mimic the BBB more accurately[33], an in-vitro system with primary human brain cells was developed by Stone and colleages[1]. Our model was based on this initial methodology and other previous models[1-3]. Further, because of supply issues and manufacture discontinuations, adjustments were needed to the previous methodology. Utilizing primary human cells is necessary as non-human primary cells are not representative of their human counterpart and exhibit substantial differences in tight junction protein properties[34, 35]. To completely recapitulate the BBB microenvironment with the associated paracellular stimuli, in-vivo constituent cells of BBB were used as primary cells in an in-vitro model employing a transwell membrane system for contact-based co-culture including neurons in non-contact (at the bottom of the well on cover slip) [36, 37]. In earlier works, various combinations of cell types, plate selection, transparency, and porosity of transwell membranes have been tested in the development of in-vitro models[25, 26, 38, 39]. Despite its static model drawback, the transwell insert-based human BBB model remains the most affordable and direct way to replicate conditions representing the BBB[40].

In this study, the 4-cell in-vitro BBB model was modified and optimized from earlier work performed by Stone and colleagues[1]. Because the specific pre-coated collagen plates utilized in Stone et al.[1] have been discontinued (Collagen coated 12 well, 3μm and 12mm inserts, Corning COSTAR, UK), we alleviated the need for these particular plates with our modified methodology. In the present work, we developed a collagen coating strategy for 12 well plates with dimensions of 12mm and 3μm pore size of the transwell membrane. In this process, polyester plates (Corning COSTAR #3462) were used to visualize cells during various stages of BBB development. The role of zinc (Zn) and serum starvation of cells have been shown to enhance the TEER value, but to our knowledge, these conditions have not

been tested in a 4-cell BBB model using primary human brain cells[41, 42]. Visualization of cells and tight junction proteins after BBB formation has always been challenging to capture with in-vitro models. In an in-vitro BBB model, the expression of tight junction proteins on the non-contact cultured neurons is unknown, though these proteins have been identified in non-BBB-associated neuronal cells. A previous study by Miyamoto and colleagues utilized knock-out mice showed the presence of tight junction protein in the myelinated axon of peripheral neuron cells[43]. Other studies have also reported the presence of claudin 5, claudin 1, and ZO-1 in ipsilateral sciatic nerve samples from legs[44, 45]. Focused investigation on the neuronal tight junction proteins would also help in understanding the BBB layer and developing cures for neuronal diseases. Researchers have also used non-human species for in-vitro BBB model development, however, given the specific complexities of the BBB, it is essential to validate the results from various species-based BBB models with a human in-vitro BBB model if these models are going to be extrapolated for clinical applications[46].

Results

TEER Measurements

Optimization of Collagen, Poly L-Lysine, and Fibronectin Coating in a Polycarbonate Transwell Membrane Containing hBMECs and Neurons. Following hBMECs and neuron cells grown in a polycarbonate transwell membrane plate, the highest TEER value of 145 ohm/cm^2 was observed when the wells were coated with collagen, poly L-Lysine and fibronectin as compared with collagen and poly L-Lysine or collagen and fibronectin as presented in Figure 2. The TEER value reduced to approximately 30 ohm/cm^2 on day eight post-seeding of cells (all coating combinations). Despite the TEER drop, these results indicate that coating with bovine collagen I, fibronectin, and Poly-L-Lysine could be a viable strategy.

Optimization of Astrocyte and Pericyte Cell Numbers in a Co-culture in Polyester Insert Membrane Improves TEER. In the polycarbonate plate, we could not observe a stable $TEER_{max}$, which could be due to different plates and the in-house coating combinations. To achieve the desired stability in $TEER_{max}$, a polyester transwell plate was used to establish the BBB model. A steady-state reading of 100 ohm/cm^2 TEER was reached and was continued for four consecutive days after reaching $TEER_{max}$. Seeding density of astrocytes and pericytes influenced the TEER value, and 0.6:0.12 million astrocytes:pericytes showed the highest TEER compared to 0.3:0.06 and 0.15:0.03 million astrocytes: pericytes (Figure 3). These results indicate that astrocytes and pericytes at the appropriate cell seeding population are essential to forming a layer with higher integrity and maximum TEER potential. Thus, further experiments were performed with 0.6:0.12 million astrocytes: pericytes.

4-Cell Model and Effect of Zn and Serum Deprivation on BBB Integrity. A steady-state TEER value in the polyester plate still showed lower values compared to previous models, indicating the need for further optimization. Various conditions, including the addition of Zn or serum to media, were used to improve TEER values. The effect of Zn supplementation, added as $ZnSO_4$, on barrier proteins expression and TEER value was measured. As depicted in Figure 4, Zn moderately increased the TEER to a maximum of 230 ohm/cm^2 (day 10)

compared to untreated controls (155 ohm/cm^2) and serum-deprived conditions (≤80 ohm/cm^2). Neurons combined with hBMECs, astrocytes, and pericytes significantly enhanced TEER demonstrating the higher integrity of the 4-cell model vs. the 3-cell BBB model (Figures 4, 5).

Imaging

Expression of Tight Junction Proteins in Astrocytes, Pericytes, and hBMECs. Expression of claudin 5 and ZO-1 proteins on the co-cultured astrocytes and pericytes at the basolateral part of the polyester transwell membrane was determined with immunostaining and analyzed with laser scanning microscopy (Figure 5a). The membrane was then probed for expression of claudin 5 and ZO-1 in the contact-cultured hBMECs in the same transwell membrane sample (Figure 5c). Both astrocytes:pericyte (Figure 5A) and hBMECs (Figure 5C) expressed claudin 5 and ZO-1 tight junctions, and their expression was increased with the addition of Zn to the medium of astrocyte: pericyte (Figure 5B) and hBMECs (Figure 5C).

Validation of Cell Types- Cellular markers for astrocytes (S100B), pericytes, and hBMECs (CD146) expressed on the cell surface were visualized with specific antibodies. In Figure 6a, astrocyte s100b are shown in red color detected with the Alexa-647 conjugated antibody, and pericytes are illuminated in green by an Alexa-488 anti-CD146 antibody. The opposite side of the same membrane was also probed for hBMECs with the Alexa-488 anti-CD146 antibody and showed CD146 expression on hBMECs (Figure 6b).

Expression of Tight Junction Proteins on hBMECs, Astrocytes, and Pericytes during Serum Deprivation and Influence of Zn Sulfate Treatment. Astrocytes: pericytes and hBMECs during serum-deprived conditions or with the addition of Zn were stained for claudin 5 and ZO-1 expression. They were not affected on ZO-1 with Zn treatment in both astrocytes: pericytes (Figure 7A vs. 7B, Column 1 and 4) and in hBMECs (Figure 7C vs. 7D, Column 1 and 4). However, Zn increased the expression of claudin 5 on astrocyte: pericyte co-cultures (Figure 7A vs. 7B, Columns 2 and 4), whereas no significant difference for claudin 5 was observed in hBMECs (Figure 7C vs. 7D, Column 2). These results indicate that astrocytes:pericytes, and hBMECs express ZO-1 and claudin 5 even during serum deprivation, and claudin 5 expression is inducible and is increased in astrocytes:pericytes during Zn sulfate treatment.

3-Cells: Astrocytes, Pericytes, hBMEC, without neurons and Poor Expression of Barrier Proteins. The sample with astrocytes and pericytes at the basolateral layer and hBMECs in the apical layer of the membrane (no neurons added) had similar ZO-1 expression as the 4-cell model but had a poor presentation of claudin 5 (Figure 8a and 8c) compared to the 4-cell model (Figure 5). Surprisingly, adding Zn did not improve claudin 5 expression when there were no neurons (Figures 8b and 8d). Cells were analyzed for their phenotype based on specific marker expressions (Figure S2).

hBMECs Monolayer with Claudin 5 and ZO-1 Expression. The hBMEC monolayer present on the transwell membrane was probed with anti-ZO-1 and anti-claudin 5 antibodies to determine expression on cells. hBMECs expressed ZO-1 and claudin 5 tight junction

proteins (Figure 9a). The image analysis shows that hBMECs alone can produce tight junction proteins; their expression is not optimal in these conditions.

Neuronal Cell with Claudin 5 Expression. In the presence or absence of neuronal cells, there was a difference in the expression of claudin 5 (Figures 5 and 8). Thus we analyzed neurons for claudin 5 expression on the neuron cell surface. We found a basal level of claudin 5 expression on neurons, and the supplementation of Zn to the medium showed a visible increase in expression (9b vs. 9c and column 4).

Fluorescence intensity measurement: We quantified the MFI of the claudin 5 protein in each represented cell from the various combinations of BBB representation. As can be seen in Figure 10a, in the presence of Zn in the media, the claudin 5 MFI of astrocyte:pericytes increased by 33%, and 43% in hBMECs. Similarly, the analysis revealed more than a 50% increase of claudin 5 MFI in astrocyte:pericyte from the 4-cell model in the absence of serum. Other BBB representations did not show any substantial difference in MFI. Neuronal cells from the 4-cell model yielded an MFI of 10, but the addition of Zn in the media increased the MFI to 19.

Functionality Testing: : DTG penetration. DTG is known to penetrate the BBB moderately[47]. As shown in Figure 10b, there is a difference of approximately 33% DTG distribution across the transwell membrane of the 4-cell model. We also found approximately 17% inhibition in drug penetration when the transwell membrane had only hBMECs monolayer without astrocyte:pericyte and without the involvement of neurons. The data also supports the idea of Zn addition to the 4-cell model for enhancing tight junction formation as the penetration of DTG through the barrier decreased by almost 48% (apical vs. basal level drug concentrations).

Discussion:

This study demonstrated a novel, reproducible, in-vitro BBB model using four primary human brain cells, illustrating a more comprehensive image analysis compared to existing BBB models. The transwell plates used by earlier groups are specific and expensive[1, 33, 48, 49]. Further, some methodology is no longer reproducible due to manufacturers' discontinuation of required supplies. Given the importance of drug permeability studies, less expensive, flexible, and reproducible transwell plate methodologies are desired. Consequently, we developed methods that utilize readily available uncoated transwell plates and standardized a strategy for developing a functional BBB in-vitro model. Although we have used the specific pore size and dimensions for the transwell membrane as discussed by Stone et al., we established ways of improving and mitigating dependence on particular aspects of their BBB model.[1] The initial visualization issue for co-cultured cells on the membrane raises uncertainty of cell attachment and growth because of poor visibility of cells when they are growing on the transwell membrane[50]. We found that polyester membranes with the same pore size of 3μm are better than polycarbonate for visual confirmation of cell adherence and growth under a microscope (Figures 2a and b). Because we used uncoated transwell membrane plates, different coating strategies were performed, and our data revealed that 50μg/ml of bovine collagen I followed

by 3μg/ml of bovine fibronectin and Poly-L-Lysine yielded the most optimal TEER values (Figure 2c). We observed $TEER_{max}$ on day six, which agreed with an earlier in-vitro primary human brain cell BBB model report[39]. However, the TEER was not static, and there was a sharp decline in TEER value after reaching $TEER_{max}$ after day six (Figure 2c)[1]. Because of unsatisfactory results from the translucent polycarbonate transwell plates, we decided to use polyester transwell plates, and its semi-transparency was better for visualization.

The best coating combination of collagen, followed by fibronectin and finally poy-L-lysine, observed with the polycarbonate membrane, was carried forward with the polyester membrane. As a standardization procedure, initially, we used only astrocyte and pericyte co-cultured with different cell seeding densities in the basolateral part of the transwell membrane. As indicated in Figure 3, the seeding density of $6x10^5$ astrocyte and $1.2x10^5$ pericyte in 150 μl exhibited TEER values nearly 2-fold greater than half of these cell densities, which is in agreement with results of earlier work[51]. Notably, the $TEER_{max}$ was established on day 6, and there was a steady state in TEER value for four consecutive days, with a drop in TEER observed on day 10 (Figure 3). A $TEER_{max}$ of ~100 ohm/cm^2 has been reported in previous studies with co-cultures of two different cell types[52, 53]. Following our standardization results and evaluation of different conditions, we developed a 4-cell in-vitro BBB model that included human primary hBMECs, astrocytes, pericytes, and neuronal cells.

According to previous reports, adding Zn and starving cells of serum media has been shown to improve TEER values in the in-vitro BBB model[41, 42]. Thus, as depicted in Figure 4, we included these conditions by adding 100 μM $ZnSO_4$ in the culture media and using media without serum. As presented in Figure 4, out of several different combinations, adding Zn increased TEER values[41]. However, we did not find enhancement of TEER in the absence of serum (i.e., starving condition); instead, we found a decrease in TEER compared to normal media. This can be explained by the need for donor-specific serum requirement for human neuronal cells[1, 54] and the use of primary cells. Our data emphasized the necessity of neurons for optimal BBB formation regardless of the presence or absence of Zn supplementation in media.

Our approach is also supported by visualizing tight junction proteins via laser scanning microscopy. Cells were visualized, and the expression pattern of tight junction proteins at both sides of the membrane (apical and basolateral sides) was analyzed without the dependence on Z-stacking, an advancement over existing in-vitro primary brain cells BBB models. It is important to note that on day 11, membranes with cells were fixed for microscopy, and by that time, there was already a decrease in TEER measurement (Figure 4). Typically, it is challenging to visualize tight junction proteins when three human primary brain cells are present on the insert membrane. Previous studies have shown tight junction protein images for a monolayer of single cell type using immortalized cells[42] or an endothelial monolayer on cellulose acetate scaffold[55]. In this study, we successfully studied the tight junction proteins ZO-1 (Zona occludens) and claudin 5 together with the identification of 4-cell types present. Confocal images of tight junction proteins ZO-1 and claudin 5 were better detected in astrocytes and pericytes when the BBB was developed in normal media with and without Zn (Figures 5a and 5b). Additionally, there was an apparent difference in claudin 5 expression on hBMECs in the presence and absence of

Zn (Figures 5c and 5d). Thus, the confocal study results supported the recorded TEER values, even though samples were preserved for microscopy on day 11 when the TEER value was in decline (Figure 4). Regarding tight junction microscopy, the previous study by Miranda-Azpiazu and colleagues imaged tight junction proteins in the multicellular BBB model, but only endothelial cells were stained for ZO-1[56]. Our present study also showed the expression of specific surface proteins using protein-specific antibodies. The individual cell type from the basolateral astrocyte:pericyte co-culture and apical hBMECs were identified with astrocyte-specific anti-S100B antibody (red), and the co-cultured pericyte along with hBMECs in the contact culture was recognized by anti-CD146 (green) antibody (Figures 6a and 6b). Initially, in the absence of serum, there was poor detection of claudin 5 on astrocytes and pericytes, as documented in Figure 7a, but the expression of claudin 5 increased in the presence of Zn (Figure 7b). No visible difference was noted for ZO-1, and similar fluorescence visibilities for claudin 5 were detected in hBMECs regardless of the presence of Zn (Figure 10a). This could be due to the potential saturation of ZO-1 or samples collected during the decline in TEER measurement (i.e., day 11). Similar to Figure 6, individual cells on both sides of the transwell membrane were confirmed (Figure S1). A study by Antje et al. presented confocal images for tight junction protein ZO-1 but not claudin 5, and the experiment was performed with human induced pluripotent stem cells (hiPSCs). In contrast, we carried out our experiment with primary cells[49]. Importantly, we investigated the role of neuronal cells in the expression of tight junction proteins with confocal microscopy. Again, no significant difference was observed for ZO-1. However, there was some improvement of claudin 5 expression in the presence of Zn (Figure 8a, 8b column 4), but the improved claudin 5 expression is better visualized for hBMECs (Figure 8c, 8d column 4). Regardless of tight junction protein expression, cells were seen intact and were successfully classified by their respective markers (Figure S2). As expected, a monolayer of hBMECs on the transwell membrane manifested tight junction proteins (Figure 9a, columns 1, 2, and 4), but the visible expression level was lower than the 4-cell model (Figure 5). Furthermore, neurons at the bottom of the wells for BBB development were also recorded for neuronal marker and claudin 5 (Figure 9b and 9c, columns 2 and 4). From the analyzed images, the basal level of claudin 5 on neuronal cells could be debatable; nevertheless, we observed a better claudin 5 distribution on the neuronal cells in the presence of supplementary Zn. Here for the first time, we are showing the confocal image of non-contact neurons from the 4-cell model exhibiting claudin 5 on its surface. There is not enough research on barrier proteins in neuronal cells. An early report by De Lorenzo and colleagues found a detectable level of claudin 5 in neurons by immunohistochemistry analysis, and the same study also suggested a better expression level of claudin 5 in astrocytes[57]. Previously mRNA analysis indicated the existence of tight junction proteins in synapses of chick ciliary ganglion[57, 58]. Though the immunohistochemistry analysis revealed a low claudin 5 in neurons[57], the studies did not perform confocal microscopy. Here, our study provides visual evidence of claudin 5 on neuronal cells from the BBB model, which can be modulated in the presence of Zn. Since all the component cells from different BBB setups exhibited similar expressions of ZO-1, we only analyzed the fluorescence intensity for the visually evident claudin 5 to confirm the level of difference. The fluorescence intensity analysis also agrees with the visually predictable difference of intensity in the presence or absence of Zn. Also, it supports the notion that neuronal

cells express claudin 5 when they are in contact with astrocytes and pericytes. (Figure 10a). Regarding specific applicability of drug penetration, we present DTG data to show functionality of the 4-cell model in regulating drug penetration into the CNS. As depicted in Figure 10, the DTG penetration data agrees with earlier findings on DTG distribution in the CNS (PMID: 24944232). This new model will allow more drugs to be studied in the future.

This article presents a simplified and effective methodology for multi-cell in-vitro BBB model development and TEER characterization completed with a comprehensive confocal microscopy confirmation. For a better understanding of the time course for the steps of model development, a flow chart has been included for the strategic time points (Figure 1). Critically, we are also showing the neuronal cells in the BBB model expressing claudin 5, which could be inducible by adding Zn micronutrient in the media. This valuable information needs further research work and validation. Going forward, our neuronal cell data from the 4-cell model can be helpful in future research work of various fields of neuroscience. The present study is part of a larger goal to analyze antimicrobial drug penetration through the BBB. Given the recent statement from the FDA to minimize in vivo animal work, this methodology will be a helpful tool for both toxicology and drug screening studies to assess penetration of various xenobiotics into the CNS. Further, incorporation of tight junction protein expression in neuronal cells of BBB model makes this work more translational (bench to bedside). We anticipate this model will better our understanding of CNS pharmacology with the ultimate goal of better patient care and clinical outcomes.

Supplementary Material

Refer to Web version on PubMed Central for supplementary material.

Funding:

We acknowledge support from the following grants from the National Institutes of Health: K23 MH125734 (to SNA) and R01 AI-124965 (to CVF). The content is solely the responsibility of the authors and does not necessarily represent the official views of the National Institutes of Health.

References

1. Stone NL, England TJ, O'Sullivan SE. A Novel Transwell Blood Brain Barrier Model Using Primary Human Cells. Front Cell Neurosci 2019; 13: 230. [PubMed: 31244605]
2. Hind WH, Tufarelli C, Neophytou M et al. Endocannabinoids modulate human blood-brain barrier permeability in vitro. Br J Pharmacol 2015; 172: 3015–27. [PubMed: 25651941]
3. Allen CL, Bayraktutan U. Antioxidants attenuate hyperglycaemia-mediated brain endothelial cell dysfunction and blood-brain barrier hyperpermeability. Diabetes Obes Metab 2009; 11: 480–90. [PubMed: 19236439]
4. Schindelin J, Arganda-Carreras I, Frise E et al. Fiji: an open-source platform for biological-image analysis. Nat Methods 2012; 9: 676–82. [PubMed: 22743772]
5. Rueden CT, Schindelin J, Hiner MC et al. ImageJ2: ImageJ for the next generation of scientific image data. BMC Bioinformatics 2017; 18: 529. [PubMed: 29187165]
6. Dyavar SR, Gautam N, Podany AT et al. Assessing the lymphoid tissue bioavailability of antiretrovirals in human primary lymphoid endothelial cells and in mice. J Antimicrob Chemother 2019; 74: 2974–8. [PubMed: 31335938]

7. Fletcher CV, Staskus K, Wietgrefe SW et al. Persistent HIV-1 replication is associated with lower antiretroviral drug concentrations in lymphatic tissues. Proc Natl Acad Sci U S A 2014; 111: 2307–12. [PubMed: 24469825]
8. Podany AT, Winchester LC, Robbins BL et al. Quantification of cell-associated atazanavir, darunavir, lopinavir, ritonavir, and efavirenz concentrations in human mononuclear cell extracts. Antimicrob Agents Chemother 2014; 58: 2866–70. [PubMed: 24614370]
9. Cecchelli R, Berezowski V, Lundquist S et al. Modelling of the blood-brain barrier in drug discovery and development. Nat Rev Drug Discov 2007; 6: 650–61. [PubMed: 17667956]
10. Liu WY, Wang ZB, Zhang LC et al. Tight junction in blood-brain barrier: an overview of structure, regulation, and regulator substances. CNS Neurosci Ther 2012; 18: 609–15. [PubMed: 22686334]
11. Stamatovic SM, Johnson AM, Keep RF et al. Junctional proteins of the blood-brain barrier: New insights into function and dysfunction. Tissue Barriers 2016; 4: e1154641. [PubMed: 27141427]
12. Dörfel MJ, Huber O. Modulation of tight junction structure and function by kinases and phosphatases targeting occludin. J Biomed Biotechnol 2012; 2012: 807356. [PubMed: 22315516]
13. Aday S, Cecchelli R, Hallier-Vanuxeem D et al. Stem Cell-Based Human Blood-Brain Barrier Models for Drug Discovery and Delivery. Trends Biotechnol 2016; 34: 382–93. [PubMed: 26838094]
14. Ghose AK, Viswanadhan VN, Wendoloski JJ. A knowledge-based approach in designing combinatorial or medicinal chemistry libraries for drug discovery. 1. A qualitative and quantitative characterization of known drug databases. J Comb Chem 1999; 1: 55–68. [PubMed: 10746014]
15. Hoshi Y, Uchida Y, Tachikawa M et al. Quantitative atlas of blood-brain barrier transporters, receptors, and tight junction proteins in rats and common marmoset. J Pharm Sci 2013; 102: 3343–55. [PubMed: 23650139]
16. Ito K, Uchida Y, Ohtsuki S et al. Quantitative membrane protein expression at the blood-brain barrier of adult and younger cynomolgus monkeys. J Pharm Sci 2011; 100: 3939–50. [PubMed: 21254069]
17. Nakagomi O, Uesugi S. [Molecular diagnosis and characterization of rotaviruses]. Rinsho Byori 1990; Suppl 85: 136–48.
18. Uchida Y, Ohtsuki S, Katsukura Y et al. Quantitative targeted absolute proteomics of human blood-brain barrier transporters and receptors. J Neurochem 2011; 117: 333–45. [PubMed: 21291474]
19. Uchida Y, Tachikawa M, Obuchi W et al. A study protocol for quantitative targeted absolute proteomics (QTAP) by LC-MS/MS: application for inter-strain differences in protein expression levels of transporters, receptors, claudin-5, and marker proteins at the blood-brain barrier in ddY, FVB, and C57BL/6J mice. Fluids Barriers CNS 2013; 10: 21. [PubMed: 23758935]
20. Syvänen S, Lindhe O, Palner M et al. Species differences in blood-brain barrier transport of three positron emission tomography radioligands with emphasis on P-glycoprotein transport. Drug Metab Dispos 2009; 37: 635–43. [PubMed: 19047468]
21. USDA National Agricultural Library. Animal Use Alternatives. available at: https://www.nal.usda.gov/animal-health-and-welfare/animal-use-alternatives.
22. FDA Modernization Act 2.0. 117th Congress. Accessed 1/31/2023. https://www.congress.gov/bill/117th-congress/senate-bill/5002.
23. Wadman M. FDA no longer has to require animal testing for new drugs. Science 2023; 379: 127–8. [PubMed: 36634170]
24. Ghaffarian R, Muro S. Models and methods to evaluate transport of drug delivery systems across cellular barriers. J Vis Exp 2013: e50638. [PubMed: 24192611]
25. Santaguida S, Janigro D, Hossain M et al. Side by side comparison between dynamic versus static models of blood-brain barrier in vitro: a permeability study. Brain Res 2006; 1109: 1–13. [PubMed: 16857178]
26. Abbott NJ, Hughes CC, Revest PA et al. Development and characterisation of a rat brain capillary endothelial culture: towards an in vitro blood-brain barrier. J Cell Sci 1992; 103 (Pt 1): 23–37. [PubMed: 1429907]
27. Pardridge WM, Triguero D, Yang J et al. Comparison of in vitro and in vivo models of drug transcytosis through the blood-brain barrier. J Pharmacol Exp Ther 1990; 253: 884–91. [PubMed: 2338660]

28. Weksler BB, Subileau EA, Perrière N et al. Blood-brain barrier-specific properties of a human adult brain endothelial cell line. FASEB J 2005; 19: 1872–4. [PubMed: 16141364]
29. Sano Y, Shimizu F, Abe M et al. Establishment of a new conditionally immortalized human brain microvascular endothelial cell line retaining an in vivo blood-brain barrier function. J Cell Physiol 2010; 225: 519–28. [PubMed: 20458752]
30. Banks WA, Kovac A, Morofuji Y. Neurovascular unit crosstalk: Pericytes and astrocytes modify cytokine secretion patterns of brain endothelial cells. J Cereb Blood Flow Metab 2018; 38: 1104–18. [PubMed: 29106322]
31. Watanabe T, Dohgu S, Takata F et al. Paracellular barrier and tight junction protein expression in the immortalized brain endothelial cell lines bEND.3, bEND.5 and mouse brain endothelial cell 4. Biol Pharm Bull 2013; 36: 492–5. [PubMed: 23449334]
32. Rist RJ, Romero IA, Chan MW et al. F-actin cytoskeleton and sucrose permeability of immortalised rat brain microvascular endothelial cell monolayers: effects of cyclic AMP and astrocytic factors. Brain Res 1997; 768: 10–8. [PubMed: 9369295]
33. Bagchi S, Chhibber T, Lahooti B et al. In-vitro blood-brain barrier models for drug screening and permeation studies: an overview. Drug Des Devel Ther 2019; 13: 3591–605.
34. Thomsen MS, Humle N, Hede E et al. The blood-brain barrier studied in vitro across species. PLoS One 2021; 16: e0236770. [PubMed: 33711041]
35. O'Brown NM, Pfau SJ, Gu C. Bridging barriers: a comparative look at the blood-brain barrier across organisms. Genes Dev 2018; 32: 466–78. [PubMed: 29692355]
36. Rauh J, Meyer J, Beuckmann C et al. Development of an in vitro cell culture system to mimic the blood-brain barrier. Prog Brain Res 1992; 91: 117–21. [PubMed: 1357719]
37. Gumbleton M, Audus KL. Progress and limitations in the use of in vitro cell cultures to serve as a permeability screen for the blood-brain barrier. J Pharm Sci 2001; 90: 1681–98. [PubMed: 11745727]
38. Booth R, Kim H. Characterization of a microfluidic in vitro model of the blood-brain barrier (μBBB). Lab Chip 2012; 12: 1784–92. [PubMed: 22422217]
39. Linz G, Djeljadini S, Steinbeck L et al. Cell barrier characterization in transwell inserts by electrical impedance spectroscopy. Biosens Bioelectron 2020; 165: 112345. [PubMed: 32513645]
40. Williams-Medina A, Deblock M, Janigro D. Models of the Blood-Brain Barrier: Tools in Translational Medicine. Front Med Technol 2020; 2: 623950. [PubMed: 35047899]
41. Shao Y, Wolf PG, Guo S et al. Zinc enhances intestinal epithelial barrier function through the PI3K/AKT/mTOR signaling pathway in Caco-2 cells. J Nutr Biochem 2017; 43: 18–26. [PubMed: 28193579]
42. Brown RC, Morris AP, O'Neil RG. Tight junction protein expression and barrier properties of immortalized mouse brain microvessel endothelial cells. Brain Res 2007; 1130: 17–30. [PubMed: 17169347]
43. Miyamoto T, Morita K, Takemoto D et al. Tight junctions in Schwann cells of peripheral myelinated axons: a lesson from claudin-19-deficient mice. J Cell Biol 2005; 169: 527–38. [PubMed: 15883201]
44. Moreau N, Mauborgne A, Bourgoin S et al. Early alterations of Hedgehog signaling pathway in vascular endothelial cells after peripheral nerve injury elicit blood-nerve barrier disruption, nerve inflammation, and neuropathic pain development. Pain 2016; 157: 827–39. [PubMed: 26655733]
45. Reinhold AK, Schwabe J, Lux TJ et al. Quantitative and Microstructural Changes of the Blood-Nerve Barrier in Peripheral Neuropathy. Front Neurosci 2018; 12: 936. [PubMed: 30618565]
46. Lippmann ES, Azarin SM, Kay JE et al. Derivation of blood-brain barrier endothelial cells from human pluripotent stem cells. Nat Biotechnol 2012; 30: 783–91. [PubMed: 22729031]
47. Letendre SL, Mills AM, Tashima KT et al. ING116070: a study of the pharmacokinetics and antiviral activity of dolutegravir in cerebrospinal fluid in HIV-1-infected, antiretroviral therapy-naive subjects. Clin Infect Dis 2014; 59: 1032–7. [PubMed: 24944232]
48. Wang Y, Wang N, Cai B et al. In vitro model of the blood-brain barrier established by co-culture of primary cerebral microvascular endothelial and astrocyte cells. Neural Regen Res 2015; 10: 2011–7. [PubMed: 26889191]

49. Appelt-Menzel A, Cubukova A, Günther K et al. Establishment of a Human Blood-Brain Barrier Co-culture Model Mimicking the Neurovascular Unit Using Induced Pluri- and Multipotent Stem Cells. Stem Cell Reports 2017; 8: 894–906. [PubMed: 28344002]
50. Kim MY, Li DJ, Pham LK et al. Microfabrication of High-Resolution Porous Membranes for Cell Culture. J Memb Sci 2014; 452: 460–9. [PubMed: 24567663]
51. Paradis A, Leblanc D, Dumais N. Optimization of an in vitro human blood-brain barrier model: Application to blood monocyte transmigration assays. MethodsX 2016; 3: 25–34. [PubMed: 26865992]
52. Daneman R, Zhou L, Kebede AA et al. Pericytes are required for blood-brain barrier integrity during embryogenesis. Nature 2010; 468: 562–6. [PubMed: 20944625]
53. Hayashi K, Nakao S, Nakaoke R et al. Effects of hypoxia on endothelial/pericytic co-culture model of the blood-brain barrier. Regul Pept 2004; 123: 77–83. [PubMed: 15518896]
54. Cestelli A, Catania C, D'Agostino S et al. Functional feature of a novel model of blood brain barrier: studies on permeation of test compounds. J Control Release 2001; 76: 139–47. [PubMed: 11532320]
55. Marino A, Baronio M, Buratti U et al. Porous Optically Transparent Cellulose Acetate Scaffolds for Biomimetic Blood-Brain Barrier. Front Bioeng Biotechnol 2021; 9: 630063. [PubMed: 33681166]
56. Miranda-Azpiazu P, Panagiotou S, Jose G et al. A novel dynamic multicellular co-culture system for studying individual blood-brain barrier cell types in brain diseases and cytotoxicity testing. Sci Rep 2018; 8: 8784. [PubMed: 29884831]
57. De Lorenzo AJ. Electron microscopy: tight junctions in synapses of the chick ciliary ganglion. Science 1966; 152: 76–8. [PubMed: 5910012]
58. Tikiyani V, Babu K. Claudins in the brain: Unconventional functions in neurons. Traffic 2019; 20: 807–14. [PubMed: 31418988]
59. Ma Q, Schifitto G, Venuto C et al. Effect of Dolutegravir and Sertraline on the Blood Brain Barrier (BBB). J Neuroimmune Pharmacol 2020; 15: 7–9. [PubMed: 31939069]
60. Gelé T, Furlan V, Taburet AM et al. Dolutegravir Cerebrospinal Fluid Diffusion in HIV-1-Infected Patients with Central Nervous System Impairment. Open Forum Infect Dis 2019; 6: ofz174. [PubMed: 31198814]

Highlights

- A cost-effective in-vitro BBB model is desired for CNS drug penetration studies
- Addition of zinc induces higher claudin 5 expressions in neuronal cells
- Dolutegravir was used to assess the functionality of the final model and cells
- Primary cells and coating strategy reduces costs and provides superior cell imaging
- 4-cell-based BBB model is suitable for the drug screening process

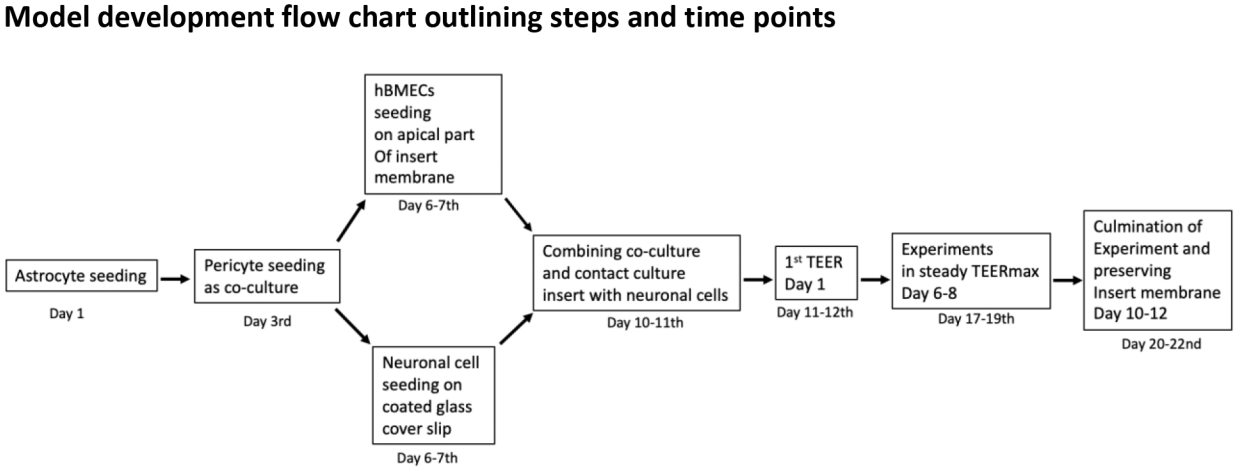

Figure 1.

Schematic representation of all critical time points and steps in the *in-vitro* BBB model development. Days represent the total days starting from astrocyte seeding until the completion of the experiment.

Abbreviations- hBMEC, Human brain microvascular endothelial cells TEER, Trans Epithelial Electrical Resistances

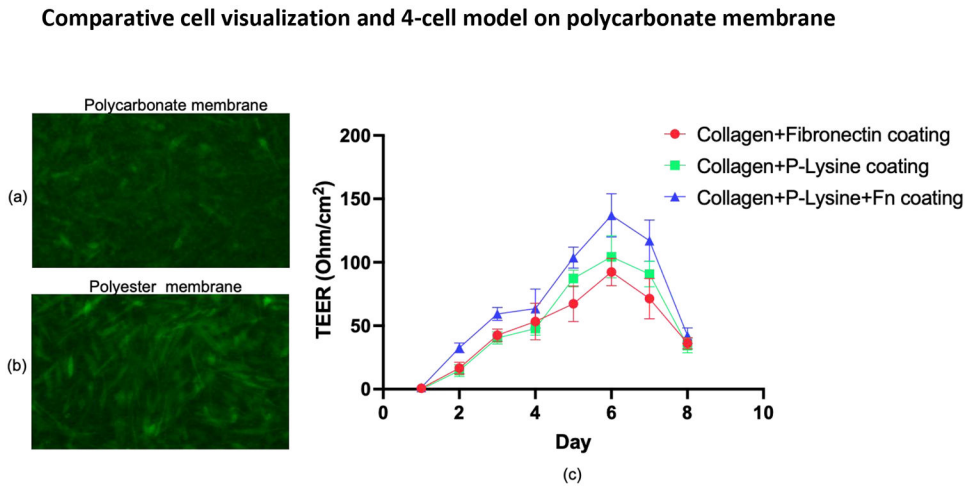

Figure 2.

Visualization of unstained cells growing on a polycarbonate (a) and a polyester (b) transwell membrane. The TEER in polycarbonate Transwell inserts was measured with an EVOM^2 meter for eight days (c). Measurement was carried out three times daily, and the average is shown. Data represent values for samples in triplicates.

Abbreviations- Fn, Fibronectin; Collagen, bovine Collagen I, and P-Lysine, Poly-L-Lysine; TEER, Trans Epithelial Electrical Resistances

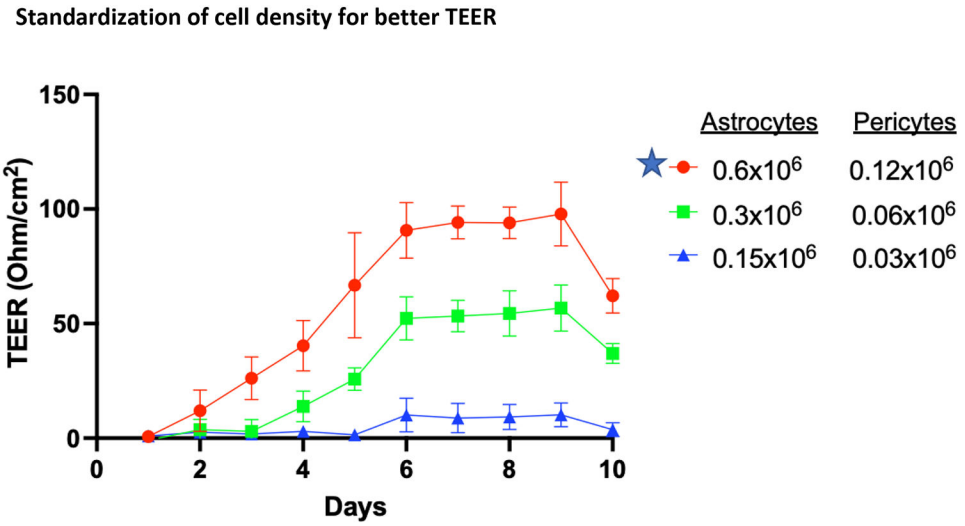

Figure 3.

TEER in astrocyte and pericyte co-cultures seeded in polyester Transwell insert. Data represent values from triplicate wells on each day for six days post-seeding. Star-marked cell density was carried forward for further experiments.

Abbreviations-TEER, Trans Epithelial Electrical Resistances

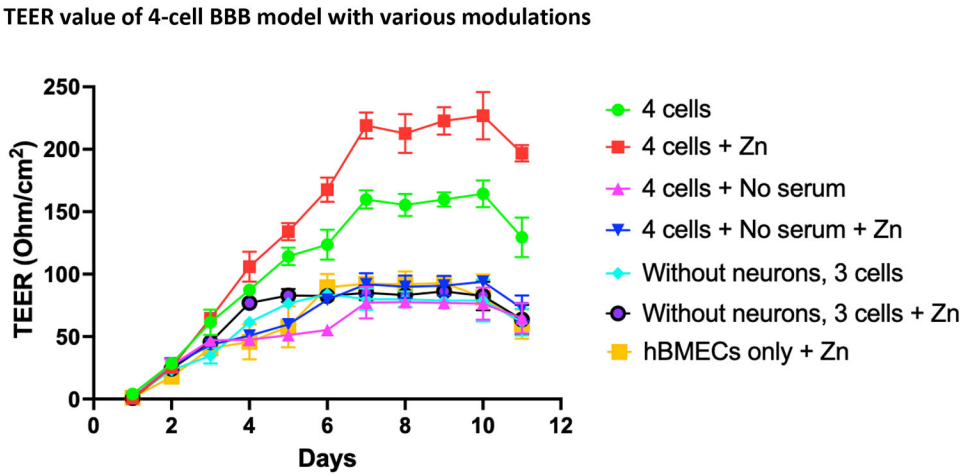

Figure 4.

TEER in 4-cell model containing hBMCEs, astrocytes, pericytes, and neurons in a polyester Transwell insert or with changing various conditions, ± Zn; ± Serum; ± neurons or only hBMECs. At each point, triplicates are used for rigor and TEER measured three times. On day 11 post-cell seeding, cells on the transwell insert membrane were fixed and preserved for confocal microscopy study.

Abbreviations-TEER, Trans Epithelial Electrical Resistances; Zn, zinc; hBMEC, Human brain microvascular endothelial cells.

Imaging cells form a 4-cell model for tight junction proteins detection.

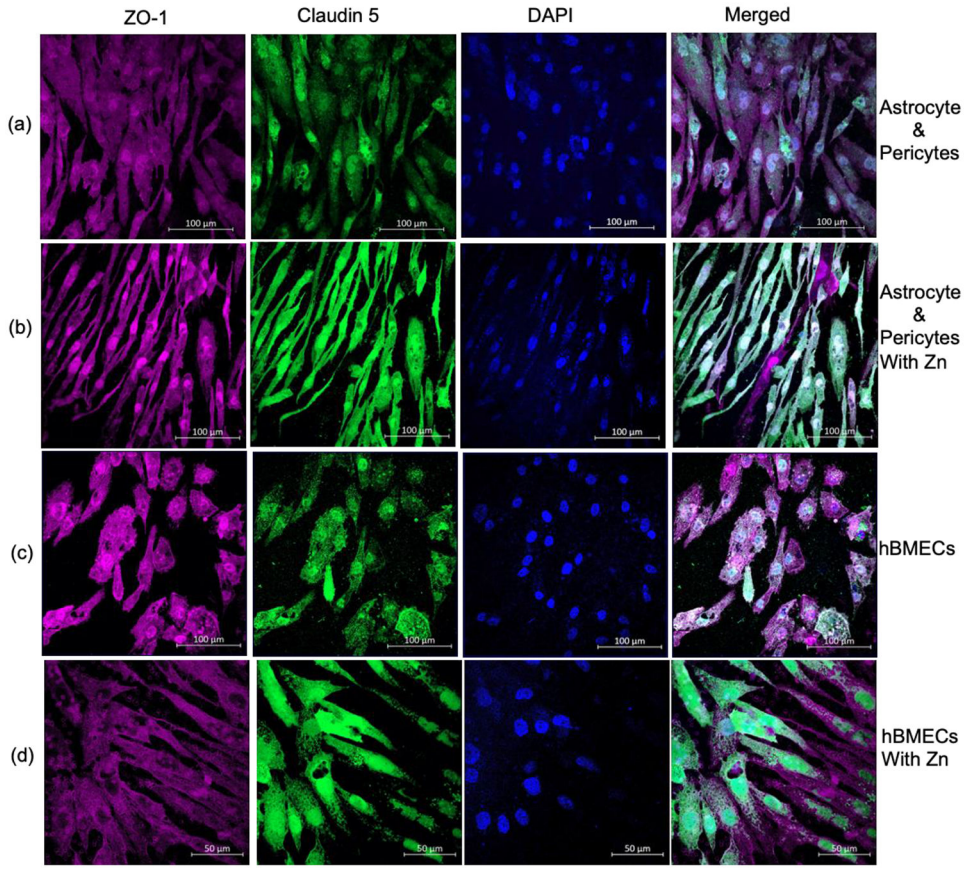

Figure 5.

Expression of TJs, ZO-1, and claudin 5 on human brain cells, layered on polyester transwell insert membrane. ZO-1 (Red) and claudin 5 (Green), and the nucleus (blue) were stained with DAPI (4,6-diamidino-2-phenylindole). TJs were observed on- astrocytes and pericytes in medium alone (a), with the addition of Zn sulfate (b), and hBMECs in medium alone (c) with Zn sulfate (d).

Abbreviations- Zn, zinc; TJ, tight junctions; Z0-1, Zona occludens; hBMCE, Human brain microvascular endothelial cells; DAPI, 4',6-diamidino-2-phenylindole.

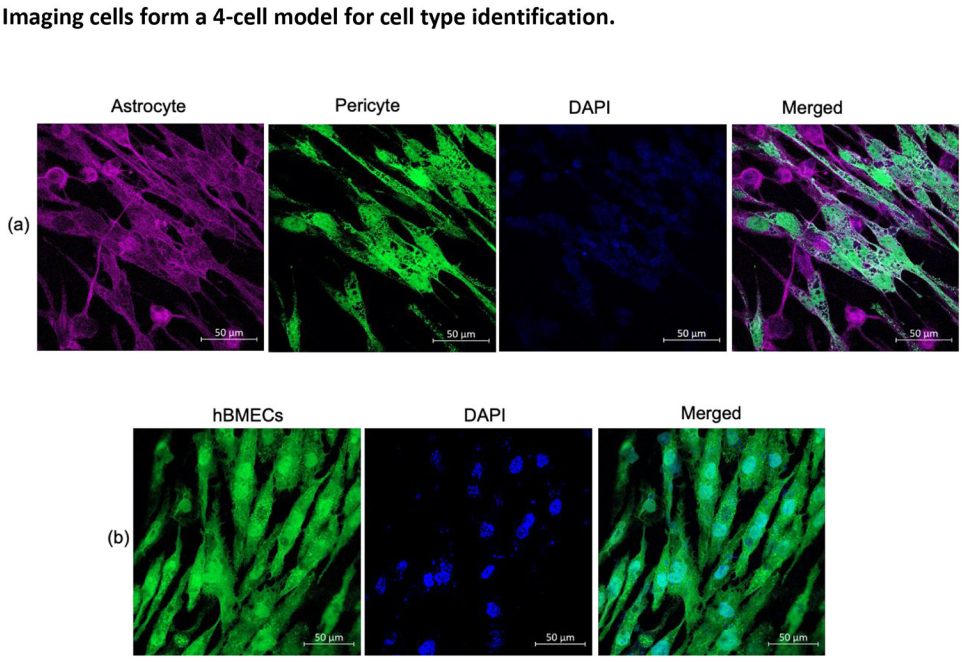

Figure 6.

Cell identification by detecting s100 beta on astrocytes and CD146 on pericytes and hBMECs as respective cell markers. Astrocytes, pericytes, and hBMEc on a transwell membrane, immunostained with a cocktail of s100beta antibody (red), an antibody against CD146 (green), and the nucleus was stained with DAPI (blue). The basolateral surface of the transwell membrane shows astrocyte and pericyte (a), and the apical part of the same transwell membrane shows hBMECs only (b).

Abbreviations- hBMEC, Human brain microvascular endothelial cells; DAPI, 4',6-diamidino-2-phenylindole.

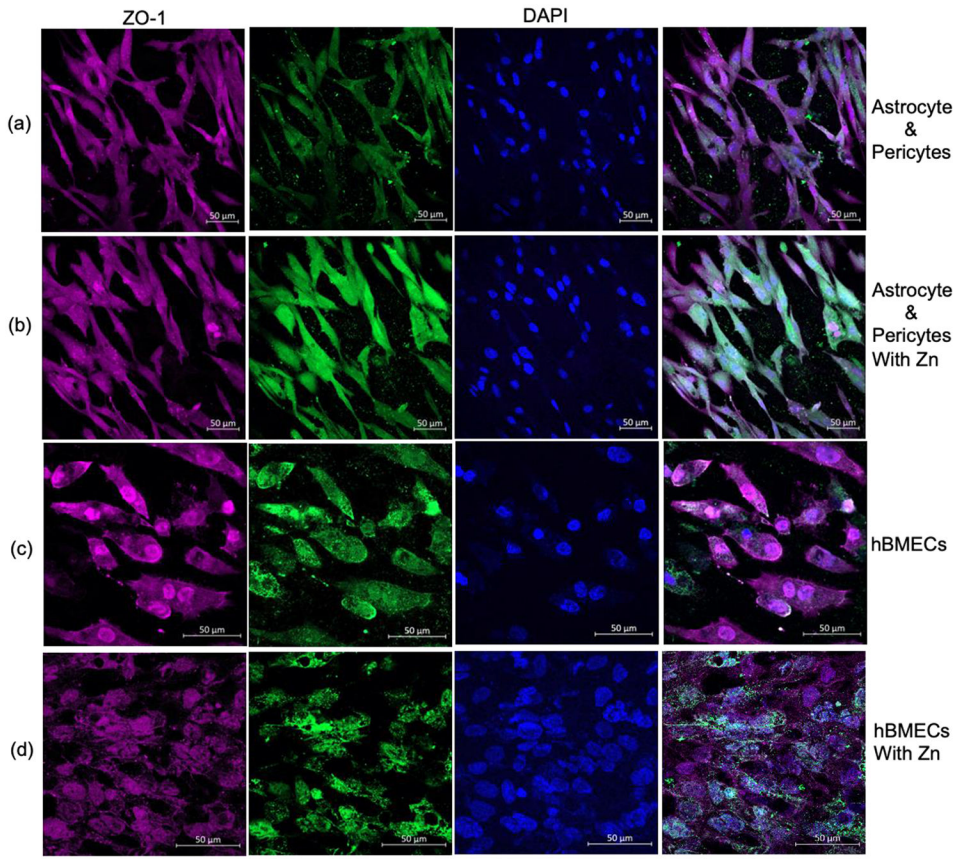

Figure 7.

Serum-free medium, confocal images of TJ protein ZO-1 (red), Claudin 5 (green) expression on astrocytes and pericytes (a) or following treatment with Zn sulfate (b) and for hBMECs (c) following treatment with Zn (d) localized to transwell insert membrane in BBB model. The nucleus was stained with DAPI.

Abbreviations- Zn, zinc; TJ, tight junctions; Z0-1, Zona occludens; hBMEC, Human brain microvascular endothelial cells; DAPI, 4',6-diamidino-2-phenylindole; BBB, blood brain barrier.

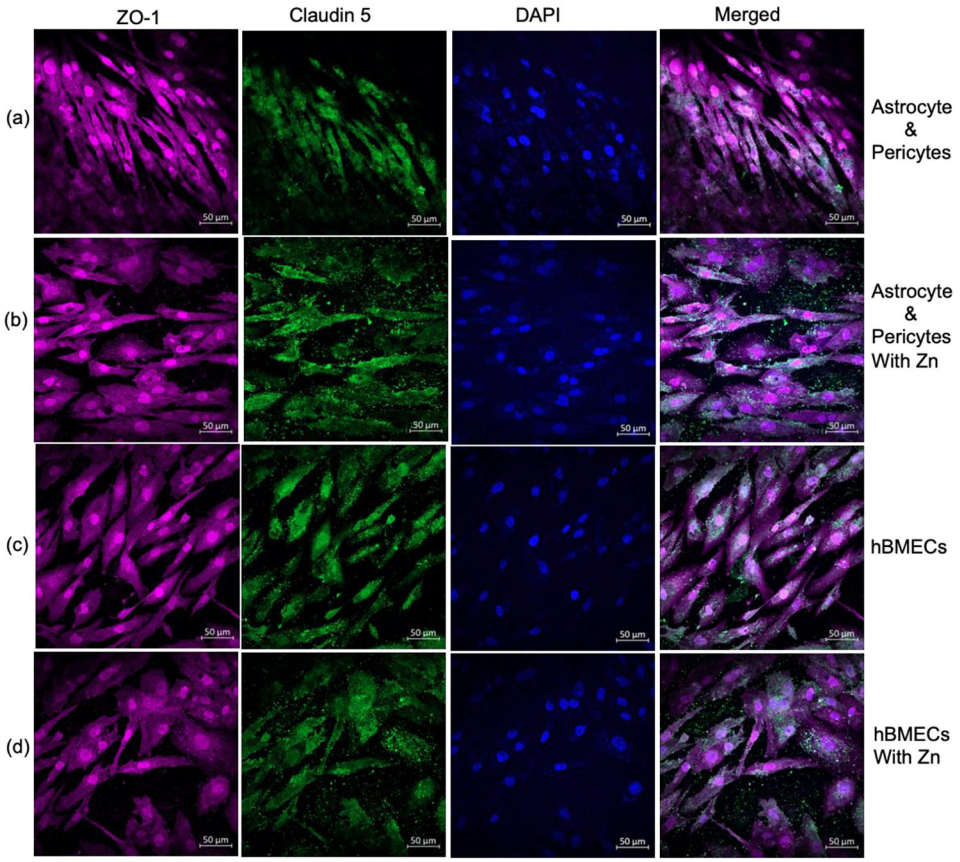

Figure 8.

In the absence of neuronal cells, expression of ZO-1 (red) and claudin 5 (green) in astrocytes and pericytes (a) and when supplemented with Zn in the medium (b) and the corresponding contact cultured hBMECs (c) supplemented with Zn (d). DAPI was used for nucleus staining.

Abbreviations- Zn, zinc; Z0-1, Zona occludens; hBMEC, Human brain microvascular endothelial cells; DAPI, 4',6-diamidino-2-phenylindole.

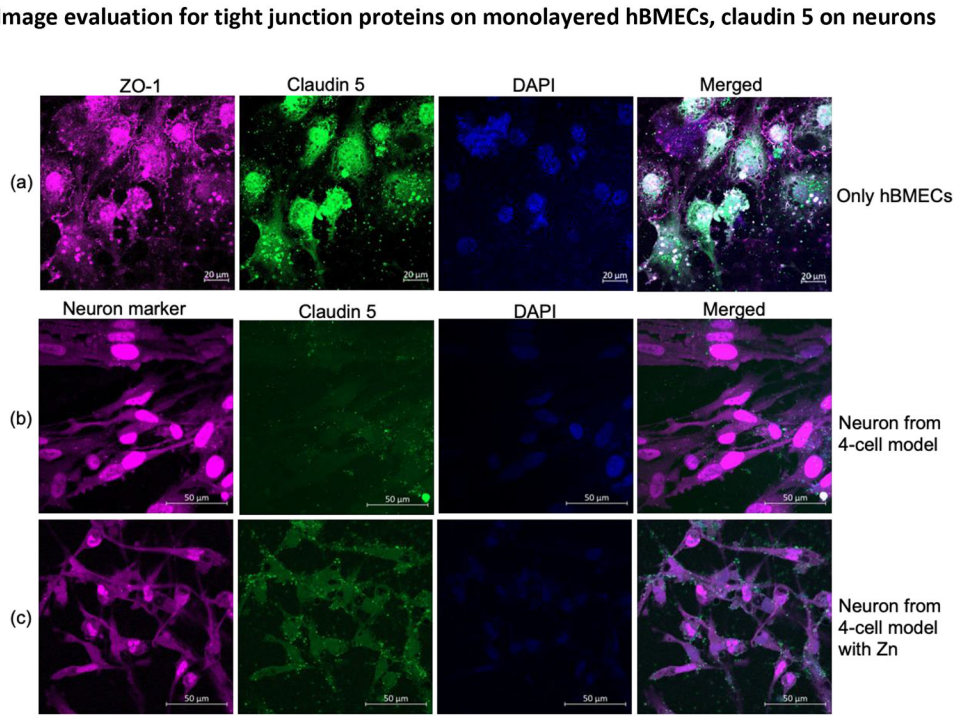

Figure 9.

Expression of ZO-1 (red), claudin 5 (green) in mono-culture of hBMECs on a transwell membrane (a) and determination of claudin 5 on neuron cell from the non-contact 4-cell model with neuronal cell marker in red (b) and when the medium for the BBB model was supplemented with Zn (c).

Abbreviations- Zn, zinc; Z0-1, Zona occludens; hBMEC, Human brain microvascular endothelial cells; DAPI, 4',6-diamidino-2-phenylindole.

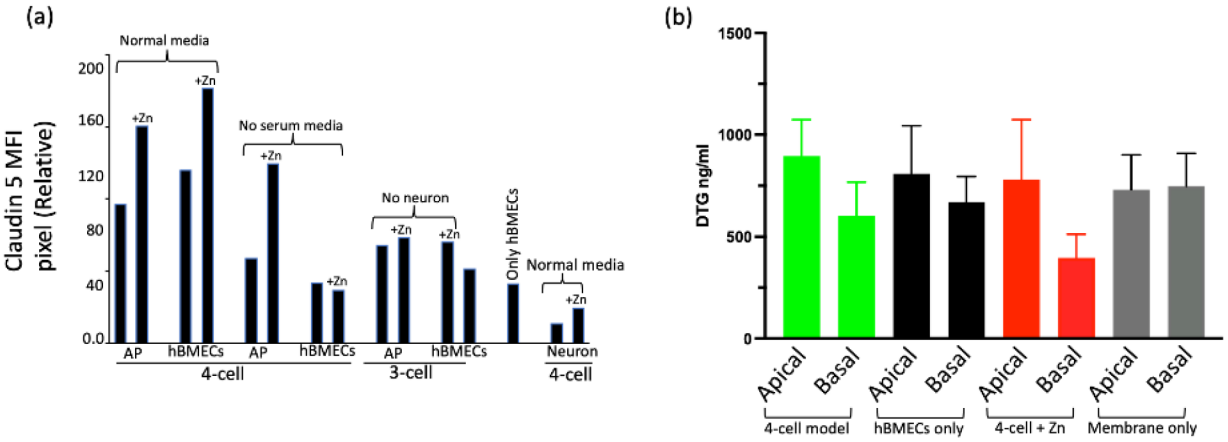

Figure 10.

Average fluorescence intensity analysis of claudin 5 for one representative corresponding to the image shown from the triplicate of BBB model types and drug penetration for different sets of BBB representation. (a) Cell surface pixel intensity for claudin 5 measured using FIJI ImageJ-win64 software and (b) evaluation of tight junction integrity and the penetration of HIV-ART drug DTG in the 4-cell model. The color-coded bar pairs show drug distribution in the apical and bottom layers of the indicated in-vitro models and control (membrane only) from a transwell membrane plate. Media from the apical and basal layer of the transwell membrane was collected after 48 hours of drug treatment. Data represent the mean concentrations from 3 replicates.

Abbreviations- MFI, mean fluorescence intensity; AP, astrocytes and pericytes; DTG, dolutegravir; hBMEC, Human brain microvascular endothelial cells; Zn, zinc